Clays and Clay Minerals, Vol. 60, No. 1, 89–98, 2012.

ROLE OF CHITIN IN MONTMORILLONITE FABRIC: TRANSMISSION ELECTRON MICROSCOPE OBSERVATIONS

JINWOOK KIM[1,*], YOKO FURUKAWA[2], KENNETH J. CURRY[3], AND RICHARD H. BENNETT[4]

[1] Department of Earth System Sciences, Yonsei University, Seoul, Korea
[2] Naval Research Laboratory, Seafloor Sciences Branch, Stennis Space Center, MS 39529, USA
[3] Department of Biological Sciences, University of Southern Mississippi, Hattiesburg, MS 39406, USA
[4] SEAPROBE, Inc., Picayune, MS 39466, USA

Abstract—Particle concentration, charge, solution chemistry (*i.e.* ionic strength), and the nature of organic matter (OM) are the major factors controlling particle flocculation in aqueous environments. In the present study, the nature of clay fabric associated with clay–OM interaction at a range of ionic strengths was the focus. In the flocculation experiments, the aqueous suspension of montmorillonite and chitin was mixed with NaCl/$MgSO_4$ electrolyte solution. Advanced sample-preparation techniques and visualization methods using transmission electron microscopy were used to observe directly the micro- and nano-scale clay–OM fabric of the resulting flocs. Such direct observation elucidated the role of OM in clay flocculation; few attempts have been made in the past due to the technical difficulties in preserving the original structure. A comparison of clay fabric at two different ionic strengths of 0 and 0.14 M revealed that the individual hexagonal clay particles settled slowly with little intra-aggregate void space (void ratio: 0.07) at 0 M while rapid flocculation and settling of clay particles at 0.14 M, with or without OM, resulted in a more open fabric with greater void space (void ratio: 0.33). The silver-staining technique demonstrated effectively the location of electron-transparent chitin in montmorillonite aggregates. Chitin appeared to link the face-to-face (FF) contacts of clay domains by bridging between negatively charged face surfaces. However, the resultant void ratio and the average hydrodynamic diameter (d_H) values were lower than in the OM-free system after flocculation. The results indicated that the interplay between ionic strength and OM content affected the floc architecture and void ratio.

Key Words—Chitin, Fabric, Flocculation, Hydrodynamic Diameter, Montmorillonite, Transmission Electron Microscopy.

INTRODUCTION

The flocculation of dispersed aqueous suspended particles and the resultant fabric are of great interest in relation to: sediment dynamics (O'Melia *et al.*, 1980; Hill, 1996); contaminant fate and transport (Pignatello and Day, 1996; Dachs and Bayona, 1997); physico-chemical characteristics such as porosity, permeability, and stress-strain behavior (Bryant and Bennett, 1988; Kim *et al.*, 2007); and sediment stability (Bennett *et al.*, 1977; Theilen and Pecher, 1991). The early concept of clay fabric developed a few typical fabric models, *e.g.* honeycomb (Terzaghi, 1925), cardhouse (Goldschmidt, 1926), turbostratic (Aylmore and Quirk, 1960), book-house (Sloane and Kell, 1966), and stairstep (O'Brien, 1971). These models were based on the observations of the shape, orientation, and arrangement of clay particles. Bennett *et al.* (1981, 1989) revealed, through numerous electron microscope observations, that the multiple unit, domain-type clay fabric (rather than the single plate concepts) was dominant in most sediments. In the early stages of fabric formation in the water column in particular, the surface electrical double layer (EDL) characteristics of the particles, in relation to the electrochemical properties of the surrounding aqueous media, exert significant control on the clay fabric (Bryant and Bennett, 1988; Bennett and Hulbert, 1986). Recent studies of flocculation modeling have found that the effect of EDL may be diminished in OM-rich sedimentary systems (Furukawa *et al.*, 2009; Mietta *et al.*, 2009).

Improvement in predictive models for scientific and technical applications in geoacoustics, geotechnique, and biogeochemistry cannot be achieved effectively without a direct investigation of the petrophysical properties of sedimentary deposits. Bennett *et al.* (1977) proposed a fabric model for smectite-rich and illite-rich clay sediments with varying void ratio (e) (= ratio of the pore volume to the volume of the solids). Based on previous laboratory analyses and theoretical considerations, the fabric of clay-rich sedimentary deposits can be affected by particle size, mineralogy, depositional environment, degree of consolidation, pore distribution, and diagenetic reactions, all of which contribute to changes and differences in geotechnical properties of sediments. The impact of physicochemical

* E-mail address of corresponding author:
jinwook@yonsei.ac.kr
DOI: 10.1346/CCMN.2012.0600108

forces on fine-grained sediments compared with the gravitational force was emphasized, particularly in early diagenetic processes (Bennett *et al.*, 1996), but such studies gave little consideration to the environmental variables such as microbe−clay interaction, organic matter (OM)−clay reaction, or temporal and spatial dynamics of redox chemistry controlled by microbial diagenesis. Recent studies have investigated particle concentration, ionic strength, and types of OM as major factors in controlling particle aggregation (Elimelech *et al.*, 1995; Gates *et al.*, 1998; Kim *et al.*, 2005; Jaisi *et al.*, 2007, 2008; Furukawa *et al.*, 2009). The mechanisms of clay−OM interaction were described by adsorption, intercalation, and cation exchange which together provided a model for the structural modification of aggregates (Lagaly, 1986; Lagaly *et al.*, 1984). Bennett *et al.* (1999, 2004) demonstrated the role of OM in the geotechnical properties of surficial marine sediments, and Curry *et al.* (2009) discussed the role and interaction of biogeochemical processes and mechanisms that drive clay nano- and microfabric development. Hulbert *et al.* (2002) demonstrated the importance of OM bridging with clay domains in observations of the sediment–water interface for selected marine and freshwater environments. Nevertheless, basic understanding of the nature of the clay fabric at the nanometer scale associated with the organo−clay interaction at various salinities remains primitive.

In the present study, the transmission electron microscopy (TEM)/Ag-staining technique (Curry *et al.*, 2007, 2009) and hydrophilic resin impregnation technique were used to minimize the structural modification in order to elucidate the clay−OM sediment fabric formed at a range of ionic strengths. Direct observation of aqueous nano-flocs (Eisma and Li, 1993; Verney *et al.*, 2009; Mietta *et al.*, 2011) has always been a challenge because many of the conventional nano-characterization techniques require sample dehydration, and the dehydration of natural aquatic clay samples inevitably alters the properties. Use of hydrophilic resin in the present study eliminated the dehydration step and greatly enhanced the potential for preservation of the original fabric for TEM observations.

MATERIALS AND METHODS

Materials and initial mixtures

The clay mineral used in this study was powdered montmorillonite ($(Na, Ca)_{1.2}(Al, Mg)_8(Si_4O_{10})_4(OH)_8 \cdot 12H_2O$; product number 46E0435, Ward's Scientific; cation exchange capacity (CEC): 110 $cmol_e/kg$; and specific surface area: 800 m^2/g). Montmorillonite is a major component of suspended clay particles in estuarine environments, and has variable surface charge or CEC compared with other clay minerals such as illite or kaolinite (Lagaly, 1986; Lagaly *et al.*, 1984; Kim *et al.*, 2005). Two grams of clay was dispersed in a 1 L distilled water column and settled for 7 h and 22 min. The supernatant containing the size fraction of <1 μm was collected by saving the upper 2.5 cm of the supernatant at 23ºC assuming 2.5 g/cm^3 average grain density and 1 centipoise (cP) of water viscosity using Stokes' Law (Batchelor, 1967). The settling and collection were repeated until a sufficient volume (50 mL) of suspension was accumulated, which was then homogenized and a 20 mL aliquot was dried and weighed to determine the suspension density. Once the suspension density was known, the remaining suspension was diluted with milli-Q water (Millipore Milli-Q Biocel Water Purification System, Massachusetts, USA) to yield a 16 mg/L suspension density.

Chitin, purified powder from crab shell (CAS 1398-61-4, Sigma), was suspended in milli-Q water to yield a 16 mg/L suspension, and then sonicated for 1 h. The chitin suspension was stored in a refrigerator and used or discarded within 72 h. Chitin is a polysaccharide and can be made visible under TEM with the TEM/Ag-staining technique (Curry *et al*., 2009).

At the beginning of each experimental run, the montmorillonite (16 mg/L) and chitin (16 mg/L) suspensions were combined with an aqueous solution containing both mono- and di-valent electrolytes (25 g NaCl + 8 g $MgSO_4 7H_2O$ to 1 L water) to yield suspension concentrations of 8 mg/L montmorillonite and 4.8 mg/L chitin, with the nominal ionic strength of 0−0.14 M. This is within typical values of suspended material concentrations found in rivers and estuaries. For example, waters from the upper estuary of Pearl River in southern Mississippi have been characterized to contain 30±20 mg/L total suspended solids (Duan and Bianchi, 2006) with 21 wt.% organic and 79 wt.% inorganic materials (R.H. Stavn, unpublished data). The average total organic carbon (TOC) concentration of 3−20 mg/L has been reported for major rivers in the U.S., including 7 mg/L for the lower Mississippi River (Reuter, 1977). After the suspensions and electrolytes were combined, the system was observed for 60 min by means of dynamic light scattering spectroscopy (DLS) using a Malvern Zetasizer nano ZS in order to determine the time-dependent size increase due to flocculation. The mixture was stirred with a magnetic stirrer in the reservoir (2.0 cm of inner diameter) with 1 revolution s^{-1} during the 60 min period, except when the optical analysis was actively taking place. Stirring ensured that the hydrodynamics was dominated by the Brownian motion and hydrodynamic shear. The exact value of the Reynolds number yielded by the magnetic stirrer is not known but can be estimated to be small (*i.e.* in the order of 10^2-10^3) from the size of the reservoir and the rotation used. The modification of floc architecture associated with stirring in the experiment was minimized. In typical estuaries the Reynolds number reaches 10^5-10^8 (Chason and Trevethan, 2006).

Embedding, thin sectioning, and silver staining techniques

The major problem with clay-fabric analysis at nano scale under TEM is the modification of the original structure due to the dehydration step required by typical sample-preparation processes. A low-viscosity resin (*e.g.* L.R. White resin) that can penetrate into the clay interlayers prevents possible layer collapse due to the dehydration, and thus maintains the original floc structure (Kim *et al.*, 1995). That technique, however, is not suitable for samples containing OM because the solvent-exchange step (methanol-water) in the L.R. White embedding procedure may remove the OM from flocs. The use of water-miscible Nanoplast resin (Leppard *et al.*, 1996) eliminates the dehydration step typically required for most TEM sample-preparation protocols, and allows the preservation of the structural integrity of the flocs throughout the sampling and embedding process (Kim *et al.*, 2005). The suspension (0.3 mL) was added to a hydrophilic Nanoplast resin, and then cured in the oven at 40ºC for 48 h (Leppard *et al.*, 1996). The cured samples were sectioned parallel to the bedding on an ultramicrotome with a diamond knife. The thin-sectioned samples were inspected carefully to ensure no damage or distortion had occurred during preparation. The 90 nm sections of resin-embedded flocs were collected on gold-coated nickel TEM grids. The silver-staining technique (Curry *et al.*, 2007) was employed to visualize the electron-transparent chitin in the flocs under TEM. Each section was oxidized with 1% periodic acid (HIO_4), floated in 1% thiosemicarbozide (TSC), and then transferred to a solution of silver proteinate. In this process, silver proteinate binds to TSC that binds to polysaccharides such as chitin. The electron dense particles of silver proteinate on the chitin can be visualized in the TEM at high magnification (Curry *et al.*, 2007). In the present study, the silver-staining with Nanoplast resin-embedding technique was shown to be an effective way of displaying the location of chitin in the montmorillonite and chitin flocs on TEM micrographs. However, precise volumetric representation of the total amount of chitin in the sample could not be provided.

Transmission electron microscopy

The floc architecture was observed at both low ($\times$10,000) and then high ($\times$100,000) magnifications in order to characterize quantitatively the spatial relationship between chitin and clay particles at the nanometer scale. The JEOL 3010 TEM operating at 300 keV with a LaB_6 filament at the Naval Research Laboratory-Stennis Space Center, Mississippi, USA, was used for all TEM analyses in the study. Hundreds of clay packets were analyzed using the negative images of TEM micrographs with a microfiche reader.

The clay-packet thickness was determined for ~159 clay packets by measuring the thickness parallel/perpendicular to c^* across grain boundaries defined by small angles to the other grains, and concentrations of edge dislocations as described previously (Kim *et al.*, 1995; Kim and Peacor, 2002). Selected area electron diffraction (SAED) patterns were also recorded to distinguish the chitin (silver particles) from the clay particles.

The void ratio was measured on the 2-dimensional (2D) TEM images taken for the flocs generated at I = 0 and 0.14 M. The ratio of total pixel counts for the void and whole area of each individual floc was determined using Photoshop® image analysis. The averaged values of void ratio at 0 and 0.14 M were obtained from the totals of 13 and nine TEM negative images, respectively, with each image containing ~6–10 void spaces. The standard deviation of each measurement (Table 1) indicated that the data points tended to be close to the mean values.

Floc-size analysis

The temporal evolution of the montmorillonite (±chitin) floc size in each system was analyzed by dynamic light scattering spectroscopy (DLS) using the Malvern Zetasizer nano-ZS at 25ºC and circumneutral pH (*i.e.* 6.5 < pH < 7.5) (Berne and Pecora, 1990). The DLS determined the average hydrodynamic diameter (d_H) of colloids and flocs suspended in liquids as follows: (1) the temporal fluctuations in the intensity of scattered light due to Brownian motion of the colloids and flocs (which is related to the size) was measured; (2) the measured scatter was expressed as a function of time (*i.e.* correlation function); (3) the cumulant-analysis fitting method was used to derive the intensity-averaged translational diffusion coefficient, D, from the correlation function; and (4) D was then used in the Stokes-Einstein equation, $d_H = k_B T/3\pi\eta D$ where k_B is the Boltzmann constant, T is the absolute temperature, and η is the viscosity of the medium, to derive d_H. Note that the 'hydrodynamic diameter' of a floc is the equivalent diameter of a spherical particle with the same Brownian motion properties as the floc. Colloid flocculation is a balance between aggregation and break-up, and the net effect of flocculation was measured. The colloids and flocs in this study were non-spherical and polydispersed. Consequently, the d_H values determined were considered not to be the true diameter but rather to be a measure of the relative average hydrodynamic diameter under the given experimental conditions. Whereas inversion methods (*e.g.* CONTIN) are often used in polydispersed systems to obtain the size distribution as well as the average particle size, the complexity of highly polydispersed and non-spherical natural colloids and flocs makes the application of inversion methods impractical. The cumulant method was, therefore, used in this study. Note also that the hydrodynamic diameters determined by DLS and reported here are the intensity average of the floc sizes.

Table 1. Hydrodynamic diameter (d_H) after 60 min and void ratio (e) with standard deviation (st.-dev.) in montmorillonite flocs at various ionic strengths.

Ionic strength (I)	— 0 M —		0.035 M	0.07 M	— 0.14 M —	
Measurements	d_H (nm)	e (st.-dev.)	d_H (nm)	d_H (nm)	d_H (nm)	e (st.-dev.)
Montmorillonite only	~200	0.07 (0.01)	~490	~1058	~1200	0.33 (0.03)
Montmorillonite + chitin mixture	~200	0.05 (0.01)	~264	~236	~600	0.22 (0.02)

The temporal evolution of the hydrodynamic diameter of montmorillonite-only and montmorillonite + chitin suspensions was determined at four different ionic strengths (*i.e.* I = 0, 0.035, 0.07, 0.14 M). From the sample reservoir (~ 20 mL), a small aliquot (*e.g.* 1 mL) of the suspension mixture was introduced to the DLS sample chamber every 2−5 min for analysis. After the analysis, the aliquot was returned to the sample chamber where it was re-homogenized with the rest of the sample suspension until the next analysis within 2−5 min.

RESULTS

Floc-size analysis by DLS

The initial hydrodynamic diameter (d_H) of montmorillonite-only flocs was $d_H \approx 200$ nm (Table 1). In the I = 0 M system, the floc size remained unchanged whereas the floc size increased to 490, 1060, and 1200 nm after 60 min in the system with greater ionic strength (*i.e.* I = 0.035, 0.07, 0.14, respectively).

The floc size showed different d_H values when chitin was present. The suspensions at I = 0 M showed very little change in the floc size (~200 nm) regardless of the presence or absence of chitin (Table 1). On the other hand, the flocculation was retarded at I = 0.035, 0.07, and 0.14 M when chitin was present, compared to the chitin-free suspensions (Table 1). The void ratio of flocculated montmorillonite was different for different ionic strength values (e = 0.07 and 0.33 for I = 0 and 0.14 M, respectively) (Table 1). Furthermore, the smaller void ratio (*i.e.* 0.22, compared to 0.33) was observed for flocs that contained chitin at I = 0.14 M.

TEM observations

The clay fabric of the montmorillonite-only systems at I = 0 and 0.14 M was examined in the TEM micrographs (Figure 1). The images indicated that individual hexagonal clay plates (H) had settled with little intra-aggregate void space (V) and some clay particles were deposited on the surface of platy clay grains (see arrowhead) at I = 0 M resulting in the small void ratio of 0.07 (Figure 1a). On the other hand, at I = 0.14 M, the various contacts of clay particles, *i.e.* face-to-face (FF), edge-to-face (EF), and edge-to-edge (EE) were developed, resulting in the large void spaces (V) with a void ratio of 0.33 (Figure 1b).

Flocs from the montmorillonite and chitin mixture at I = 0 and 0.14 M were also examined in the TEM micrographs (Figure 2). The samples shown were not treated with the silver-staining technique and so chitin was not visible. The images were compared with the silver-stained images to illustrate the advantage of using the silver staining. The TEM micrographs of montmorillonite and chitin mixture showed few flocculation features at I = 0 strength (*i.e.* lacking the range of FF, EF, and EE structures). Instead the individual clay particles settled with FF contacts (see the outlined magnified area) due to the lack of flocculation while in the water column and subsequent settling of individual discrete particles. This resulted in a few small void spaces (V) with a void ratio of e = 0.05 (Figure 2a). When the ionic strength was 0.174 M, flocculation in the water column occurred and increased the clay particle linkages creating a number of large void spaces (V) with a void ratio of e = 0.22 (Figure 2b).

The packet-size distribution for the montmorillonite-only and the montmorillonite + chitin mixture was measured on the TEM micrographs. The term 'packet' refers to discrete domains with coherent layers of montmorillonite separated from other domains by small angles (dislocations) or contrast (Kim *et al.*, 1995; Kim and Peacor, 2002). For example, a TEM micrograph of clay flocs at I = 0.14 M with the EE, EF, and FF contacts (outlined area in Figure 3a) was magnified to measure the size distribution of discrete clay packets (Figure 3b). Each clay floc comprised several clay packets identified by coherent lattice fringes with angles/dislocations (areas 1, 2, and 3) and contrast changes (areas 4 and 5) on the TEM lattice-fringe image (Figure 3b). The thickness of each packet was measured by counting the number of the layer spacings (~1.1−1.2 nm/spacing) in each montmorillonite packet on the TEM micrograph at a high magnification as shown in the inset to Figure 3b. The expansion of montmorillonite layers induced by chitin intercalation into the interlayer was not observed on TEM lattice fringes. The packet size of 83 and 76 clay domains in pure montmorillonite as well as montmorilonite + chitin systems at the same ionic strength (0.14 M) were determined to have mean values of 14.3 nm (standard deviation = 0.9 nm) and 13.8 nm (standard deviation = 0.8 nm), respectively, showing a similar packet-size distribution for both systems (Figure 4).

In order to elucidate the role of chitin in clay fabrics, the TEM micrographs of silver-stained chitin and montmorillonite mixture at I = 0.14 M were examined (Figure 5). Clay particles (Mont.) formed domains and

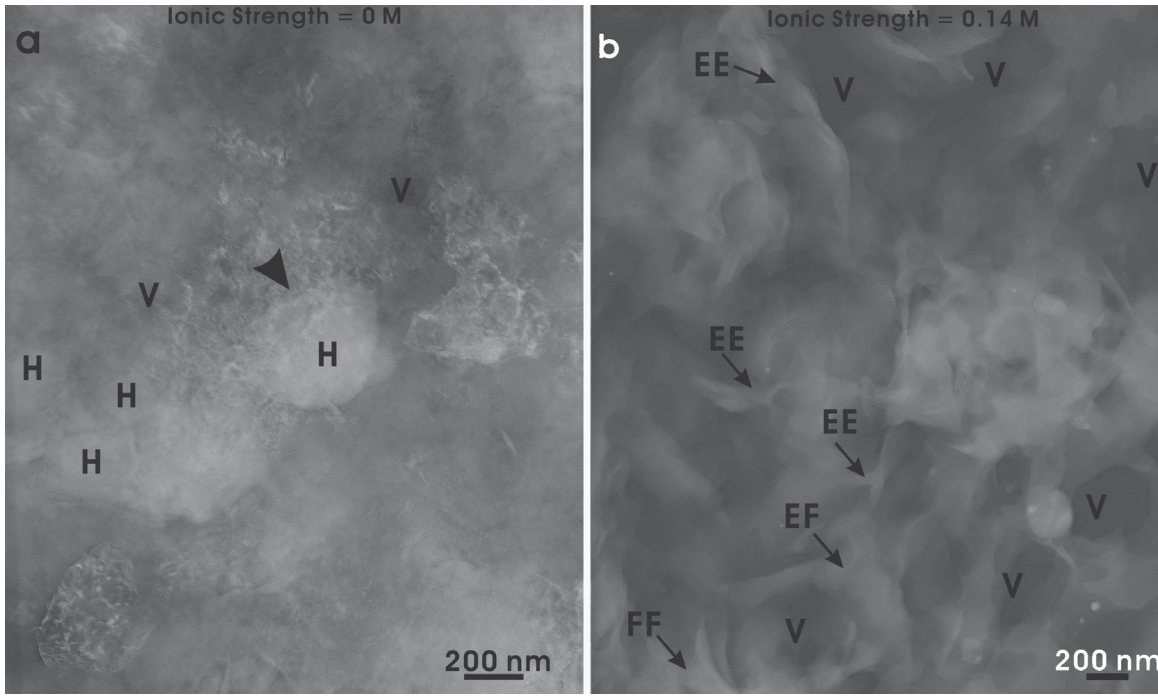

Figure 1. TEM images of montmorillonite-only suspensions at (a) $I = 0$ M and (b) $I = 0.14$ M. Individual hexagonal clay particles (H) settled without flocculation, resulting in little intra-aggregate void space (V) with a void ratio of 0.07 observed at $I = 0$ M. Various contacts (EE, EF, and FF where EE = edge to edge, EF = edge to face, and FF = face to face) of clay domains at $I = 0.14$ M resulted in a large void space (V) with a void ratio of 0.33.

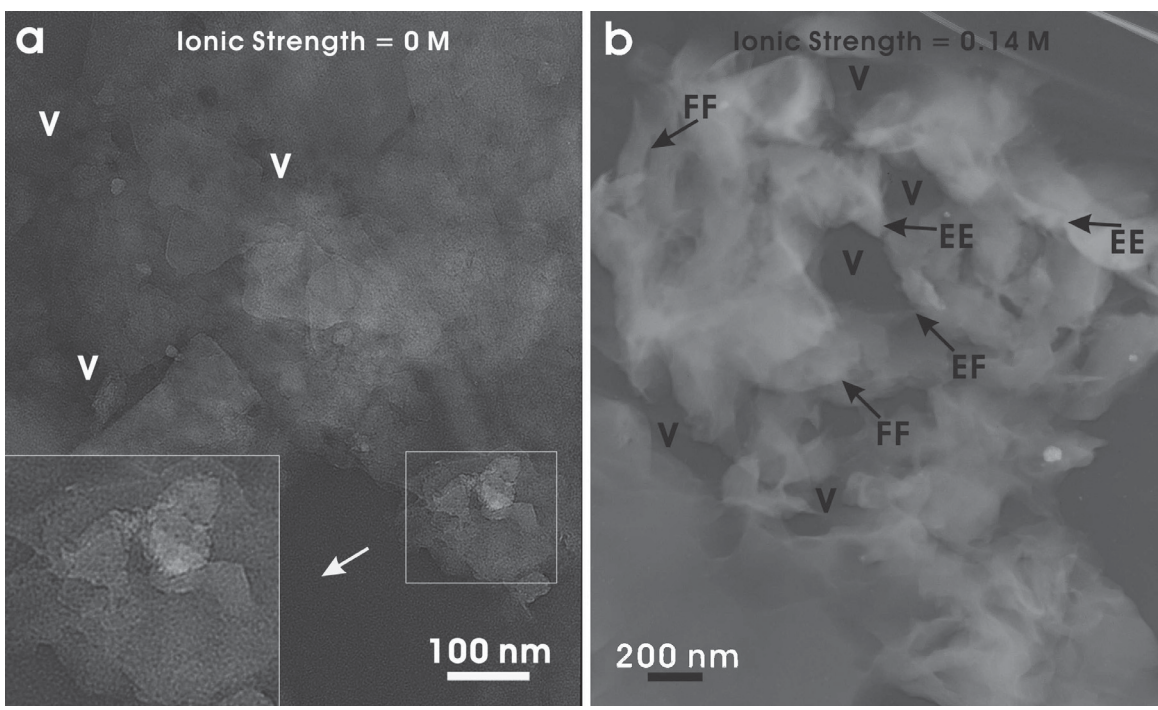

Figure 2. TEM images of montmorillonite and chitin mixtures at (a) $I = 0$ M and (b) $I = 0.14$ M. Flocculation features were not observed at $I = 0$ M; rather the individual clay particles settled in a face-to-face fabric signature (see outlined, magnified area) resulting in small void spaces (V) with a void ratio of 0.05. The flocculations at $I = 0.14$ M caused the large void spaces (V) with a void ratio of 0.22 associated with clay-particle linkages (FF, EF, and EE contacts where EE = edge to edge, EF = edge to face, and FF = face to face).

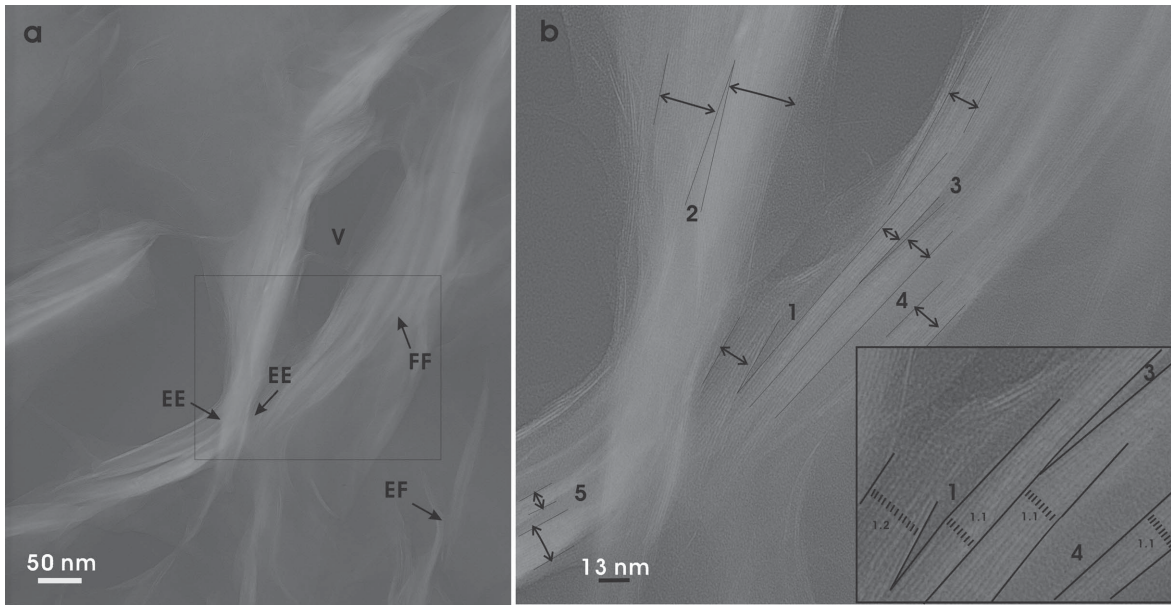

Figure 3. TEM images of montmorillonite and chitin mixtures at $I = 0.14$ M (a) at low magnification showing EE = edge to edge, EF = edge to face, and FF = face to face contacts and (b) lattice fringes (1.1−1.2 nm spacing) of discrete clay packets at high magnification. Each clay floc consisted of several clay packets identified by coherent lattice fringes with angles/dislocations (*e.g.* areas 1, 2, and 3) and contrast changes (*e.g.* areas 4 and 5) on the TEM lattice-fringe image.

each domain was linked by chitin, resulting in the 'globule'-shaped organo-clay clusters with large (~300 nm) void spaces (V) (Figure 5a). Each of the bridged clay domains formed perfect stacks (Figure 5b). The silver nanoparticle clusters (fine black dots indicated by arrows in the TEM micrographs [Figure 5c,d] of the outlined areas in Figure 5a,b, respectively) indicated the location of chitin in clay fabrics. The black dots observed in chitin and montmorillonite-dominated areas were confirmed by SAED patterns with the three strongest silver Bragg reflections of 0.24, 0.20, and 0.12 nm and diffused d_{002} reflections of montmorilonite (inset in Figure 5b).

DISCUSSION

Clay fabric

In the montmorillonite-only system, the degree of clay flocculation and void-space formation depended on the difference in ionic strength (Table 1). The wide variety of clay-particle contacts at I = 0.14 M (Figure 1b) was generated as a result of rapid flocculation, resulting in the large void ratio. On the other hand, the lack of water-column flocculation at I = 0 M inhibited the void formation (Figure 1a). In the montmorillonite-only systems, the EDL of the montmorillonite surfaces with the increased ionic strength, resulted in the compressed EDL and the electrostatic repulsive

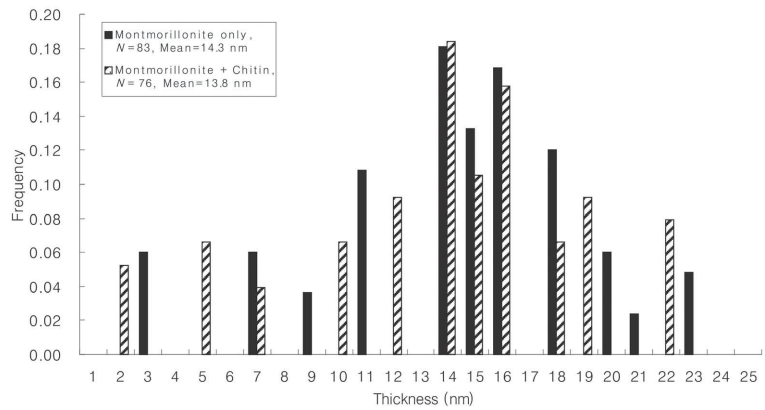

Figure 4. Discrete clay-packet-size distribution of montmorillonite only and of a montmorillonite + chitin mixture at $I = 0.14$ M. The TEM thicknesses of 83 and 76 individual clay packets in each suspension were measured perpendicular to c^* across grain boundaries on the microfiche reader resulting in mean thicknesses of 14.3 nm and 13.8 nm, respectively.

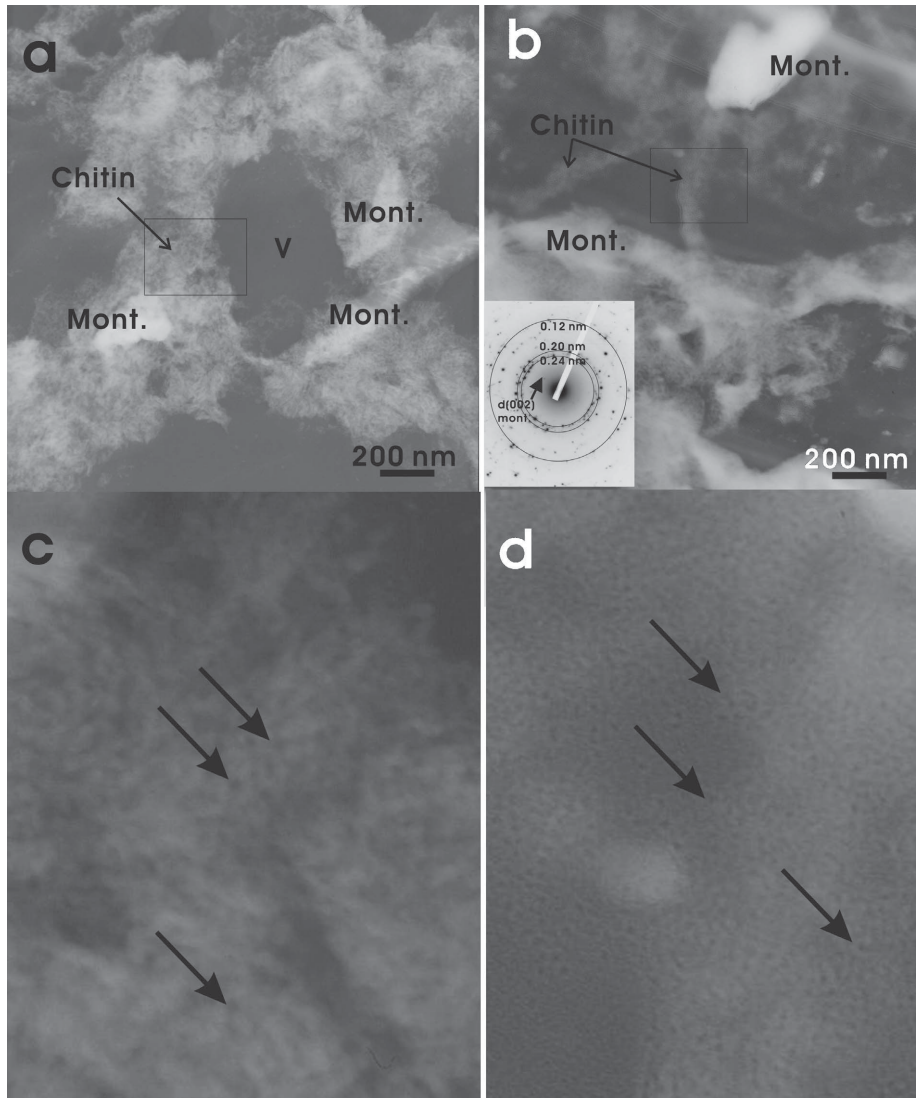

Figure 5. TEM images of montmorillonite and of a silver-stained chitin mixture at $I = 0.14$ M revealing the role of biopolymers in clay flocculation. The silver aggregates are located in the chitin (black dots indicated by arrows). Chitin (a) surrounded the clay particles creating large 'globular' organo-clay clusters with large void space (V) and (b) bridged the discrete clay packets with face-to-face (FF) contact. The inset figure shows the SAED pattern of the montmorillonite-chitin mixture with diffuse ring patterns of amorphous chitin and d_{002} spacing of montmorillonite clays with the three strongest silver Bragg reflections of 0.24 nm, 0.20 nm, and 0.12 nm confirming the silver-stained chitin. The outlined areas in parts a and b were magnified and the aggregates of silver (black dots) locating chitin were marked by arrows (c and d).

forces combined with energy mechanisms (*e.g.* thermo-kinetics) were able to increase flocculation (Bennett and Hulbert, 1986). The variable edge charges of clay particles or exchanging structural OH- groups (Lagaly *et al*., 1984) may also induce flocculation.

In the montmorillonite + chitin systems, however, flocculation was not as prominent as in the mont-morillonite-only systems suggesting that the addition of chitin increased the net repulsive forces between mont-morillonite surfaces. The zeta potential, which can be considered as the proxy for the surface potential and is directly related to the EDL repulsive forces, was analyzed recently for both montmorillonite and chitin (Furukawa *et al.*, 2009). The results showed that montmorillonite surfaces are far more electronegative than chitin surfaces at all ionic strength values (Furukawa *et al.*, 2009) relevant to the present study. In other words, if the flocculation behavior were to be dominated by the EDL repulsion, the montmorillonite-chitin systems would flocculate more readily than the montmorillonite-only systems. The nature of this addi-tional repulsion other than EDL repulsive forces (non-DLVO repulsive forces) could explain the contrary observation.

Although chitin increases the net repulsive force, it does not prevent flocculation entirely. Montmorillonite + chitin systems flocculate at high ionic strength, albeit more slowly than the montmorillonite-only systems. The TEM micrographs suggest that chitin may be more likely to act as a bridge between the clay particles during flocculation. Indeed, the clay particle flocculation at I = 0.14 M caused the various clay-domain contacts (Figure 2b) resulting in the large void spaces, while the lack of rapid flocculation and subsequent slow settling of unflocculated clay domains at I = 0 M (Figure 2a) led to small void spaces, as reflected in the changes in the values of d_H and void ratio (Table 1). Chitin appeared to link the FF contacts of clay domains at I = 0.14 M which would otherwise be repulsive due to the negative surface charge. Divalent cations are more effective than monovalent ions at causing EDL to shrink. The expansion of montmorillonite layers associated with the intercalation of OM into clay interlayers (Vali and Hesse, 1990; Lagaly, 1981) was not detected in the TEM lattice-fringe images. This may be due to the high ionic strength at which the adsorption of OM to clay surfaces is the dominant mechanism compared with other interactions such as intercalation and cation exchange (Lagaly *et al.*, 1984). The chitin bridging the montmorillonite domains was clearly observed in the TEM micrographs for the silver-stained sample (Figure 5) and the resultant void ratio and d_H values were shown to be reduced compared to the chitin-free systems (Table 1). At I = 0.14 M in particular, the architecture of the flocs showed various organo-clay fabric resulting from chitin and montmorillonite interaction, *e.g.* 'globule shape' where each clay domain was linked by chitin (Figure 5). The various particle contacts (EE, FF, and EF) associated with the rapid flocculation at high ionic strength created the globular aggregates.

Void ratio and d_H

The void ratios reported here (Table 1) were measured on the 2D TEM images. The 2D determination of void ratio is more accurate on randomly arranged fabrics than on fabrics with a preferred orientation (Bennett *et al.*, 1989). The void ratios based on 2D serial images that were then reconstructed as a 3D fabric representation showed the same results as with 2D measurement (unpublished data). Caution is required, however, when interpreting the void ratio because the floc architecture could be modified by the break-up of flocs during sample preparation. For the present study, the thin-sectioning was done parallel to the sediment bedding, minimizing the amount of microtome-related artifacts. The packet-size distributions at I = 0.14 M were similar in both montmorillonite-only and montmorillonite + chitin systems (Figure 4) indicating that the initial formation of individual clay packets in suspensions where I = 0.14 M were not modified by the intercalation of chitin (Figure 4). Therefore, the changes in d_H value and void ratio were mainly associated with the flocculation of clay rather than the intercalation of chitin over a range of ionic strength. Note, however, that the hydrodynamic diameter determined by the DLS method may not agree with the TEM-observed floc sizes due to the very definition of the 'hydrodynamic diameter.' However, the relative trend agrees (*i.e.* the average floc size is largest in the high ionic-strength system with no chitin).

Implications for the natural environment

The present study showed that the open fabric with various clay associations (*i.e.* FF, FE, and EE) can be formed very rapidly when the solution containing the colloidal suspension of clays and OM encounters water with high electrolyte concentrations (*e.g.* seawater). Even though chitin is an important source of ocean and estuarine OM (Johnstone, 1908; Boyer and Kator, 1985), the chitin concentrations of the <0.2 μm clay fraction in Delaware Bay ranged from 4 to 21 mg/L (Montgomery *et al.*, 1990). The low concentration of chitin in the water column may be due to the physical behavioral partitioning (fast sinking, microbial utilization, or trapping in the clay) expected of the nearly electroneutral chitin colloids.

The intimate spatial association between clay surfaces and chitin molecules (Figure 5) was formed very rapidly in I = 0.14 M systems, within ~60 min or less of the encounter between montmorillonite and chitin. This observation may be applicable to our understanding of the theoretical modeling (Hill *et al.* 2001; Furukawa *et al.*, 2009) and modification of petrophysical properties of the sediments in natural environments (Bryant and Bennett, 1988; Bennett and Hulbert, 1986). However, the observed type of particle association in the present study may not be same in the natural environment, because the variabilities of grain size, compaction, bioavailability of OM, microbe−mineral interaction, and particle-to-particle aggregation, in addition to the clay−OM interaction, make it difficult to predict the resultant sediment fabric and its petrophysical properties. For example, marine sediments with $\geqslant$3−4% TOC have greater porosities and void ratios than similar fine-grained sediments (same grain size and mineralogy) with very little OM ($\leqslant$3% TOC) (Bennett *et al.*, 1999, 2004). Furthermore, the chitin or other OM with positive charge or polarity will be attracted preferentially to the regions of minimum potential energy formed by clay-fabric signatures (EF, FF, and EE domain contacts). Therefore, clay−OM interaction is not simply a function of the negative surface charge of the clay component but depends also on the chemical composition, shape, and size of the OM (Bennett and Hulbert, 1986). Direct TEM observation of flocs associated with clay−OM interaction resulting in the modification of void ratio call for further study of clayey sediment fabric in natural clay-water systems, particularly OM-rich environments.

SUMMARY

A rapid aggregation and settling of colloidal clays in high ionic-strength solutions resulted in large flocs with very open (*i.e.* large intra-floc void ratio) fabric whereas the lack of aggregation and eventual slow settling of individual clay particles in low ionic-strength solutions led to clay fabric with very small void ratios. Chitin retarded, but failed to prevent entirely, the flocculation of montmorillonite (Table 1). The TEM analysis revealed that the small aggregates that formed in the chitin-containing systems had an open structure (void ratio = 0.22) with chitin bridging two negatively charged montmorillonite surfaces to yield the FF contacts. The interplay between ionic strength and OM content affected the floc architecture and void ratio. The silver-staining technique with Nanoplast resin embedding was shown to be an effective way of locating chitin in montmorillonite fabrics using TEM.

ACKNOWLEDGMENTS

The research described here was supported by the Basic Science Research Program through the National Research Foundation of Korea (NRF) funded by the Ministry of Education, Science, and Technology (20110013407) to Jinwook Kim, ONR/NRL Core 6.1 funding (PE#0601153N) to Yoko Furukawa, and was partially supported by grants from the National Science Foundation to R. Bennett (OCE-0824566 and OCE-0930685) and K. Curry (OCE-0824569 and OCE-0930879).

REFERENCES

Aylmore, L.A.G. and Quirk, J.P. (1960) Domain or turbostratic structure of clay. *Nature*, **187**, 1046–1048.

Batchelor, G.K. (1967) *An Introduction to Fluid Dynamics*. Cambridge University Press, Cambridge, UK.

Bennett, R.H., Bryant, W.R., and Keller, G.H. (1977) Clay fabric and geotechnical properties of selected submarine sediment cores from the Mississippi Delta. U.S. Department of Commerce-NOAA-ERL Publication, NOAA Professional Paper, 9:86.

Bennett, R.H., Bryant, W.R., and Keller, G.H. (1981) Clay fabric of selected submarine sediments: Fundamental properties and models. *Journal of Sedimentary Petrology*, **51**, 217–232.

Bennett, R.H. and Hulbert, M.H. (1986) Clay Microstructure. International Human Resources Development Corporation, Boston, USA, 161 pp.

Bennett, R.H., Fischer, K.M., Lavoie, D., Bryant, W.R., and Rezak, R., (1989) Porometry and fabric of marine clay and carbonate sediments: determinants of permeability. *Marine Geology*, **89**, 127–152.

Bennett, R.H., Hulbert, M.H., Meyer, M.M., Lavoie, D.M., Briggs, K.B., Lavoie, D.L., Baerwald, R.J., and Chiou, W.A. (1996) Fundamental response of pore water pressure to microfabric and permeability characteristics: Eckernforde Bay. *Geo-Marine Letters (special issue)*, **16**, 182–188.

Bennett, R.H., Ransom, B., Kastner, M., Baerwald, R.J., Hulbert, M.H., Sawyer, W.B., Olsen, H., and Lambert, M.W. (1999) Early Diagenesis: Impact of Organic matter on Mass Physical Properties and Processes, California Continental Margin. *Journal of Marine Geology*, **159**, 7–34.

Bennett, R.H., Lambert, M.W., Hulbert, M.H., Curry, C.W., Olsen, H.W., and Lowrie, A. (2004) Microfabric and Organic Matter Impact on Burial Diagenesis From Mud to Shale. Siltstones, Mudstones and Shales: Depositional Processes and Reservoir Characteristics, SEPM-AAPG Special Symposium Short Course **9**, available on CD through SEPM.

Berne, B.J. and Pecora, R. (1990) *Dynamic Light Scattering*. Krieger Publishing Company, Malabar, Florida, USA.

Boyer, J.N. and Kator, H.I. (1985) Method for measuring microbial degradation and mineralization of ^{14}C-labeled chitin obtained from the blue crab, *Callinectes sapidus. Microbial Ecology*, **11**, 185–192.

Bryant, W.R. and Bennett, R.H. (1988) Origin, physical, and mineralogical nature of red clays: the Pacific basin as a model. *Geo-Marine Letters*, **8**, 189–249.

Chason, H. and Trevethan, M. (2006) Turbulence in a small subtopical estuary with semi-diurnal tides. Proceedings of the 2nd International Conference on Estuaries and Coasts (ICEC-2006), Guangzhou, Guangdong Province, China. Guangdong Economy Publishers, Vol. 1 (ISBN 7-80728-422-6).

Curry, K.J., Bennett, R.H., Mayer, L.M., Curry, A.L., Abril, M., Biesiot, P., and Hulbert, M.H. (2007) Direct visualization of clay microfabric signatures driving organic matter preservation in fine-grained sediment. *Geochimica et Cosmochimica Acta* **71**, 1709–1720.

Curry, K.J., Bennett, R.H., Smithka, P.J., and Hulbert, M.H. (2009) Hierarchical modeling of biogeochemical processes and mechanisms that drive clay nano- and microfabric development. Pp. 287–317 in: *New Nanotechniques* (A. Malik and R.J. Rawat, editors). Nova Science Publishers, Inc., Hauppauge, New York, USA.

Dachs, J. and Bayona, J.M. (1997) Large volume preconcentration of dissolved hydrocarbons and polychlorinated biphenyls from seawater. Intercomparison between C18 disks and XAD-2 column. *Chemosphere* , **35**, 1669–1679.

Duan, S.W. and Bianchi, T.S. (2006) Seasonal changes in the abundance and composition of plant pigments in particulate organic carbon in the lower Mississippi and Pearl Rivers. *Estuaries and Coasts*, **29**, 427–442.

Eisma, D. and Li, A. (1993) Changes in suspended-matter floc size during the tidal cycle in the Dollard estuary. *Netherlands Journal of Sea Research*, **31**, 107–117.

Elimelech, M., Gregory, J., Jia, X., and Williams, R.A. (1995) *Particle Deposition and Agglomeration: Measurement, Modeling and Simulation.* Butterworth-Heinemann Ltd, UK.

Furukawa, Y., Watkins, J.L., Kim, J.-W., Curry, K.J., and Bennett, R.H. (2009) Aggregation of montmorillonite and organic matter in aqueous media containing artificial seawater. *Geochemical Transactions*, **10**, 2.

Gates, W.P., Jaunet, A., Tessier, D., Cole, M.A., Wilkinson, H.T., and Stucki, J.W. (1998) Swelling and texture of iron bearing smectites reduced by bacteria. *Clays and Clay Minerals*, **46**, 487–497.

Goldschmidt, V.M. (1926) Undersokelser over lersedimenter. *Nordisk Jordbrugs forskuing*, **4–7**, 434–445.

Hill, P.S. (1996) Sectional and discrete representations of floc breakage in agitated suspensions. *Deep Sea Research*, **I 43**, 679–702.

Hill, P.S., Voulgaris, G., and Trowbridge, J.H. (2001) Controls on floc size in a continental shelf bottom boundary layer. *Journal of Geophysical Research-Oceans*, **106**, 9543–9549.

Hulbert, M.H., Bennett, R.H., Baerwald, R.J., Long, R.L., Curry, K.J., Curry, A.L., and Abril, M.T. (2002) Observations of the sediment-water interface: Marine and fresh water environments. *Marine Georesources and Geotechnology*, **20**, 255–274.

Jaisi, D.P., Dong, H., Kim, J.-W., He, Z., and Morton, J. (2007) Nontronite particle aggregation induced by microbial Fe(III)

reduction and exopolysaccharide production. *Clays and Clay Minerals*, **55**, 98–109.

Jaisi, D.P., Shanshan, J., Dong, H., Blake, R.E., Eberl, D.D., and Kim, J.-W. (2008) Role of microbial Fe(III) reduction and solution chemistry in aggregation and settling of suspended particles in the Mississippi River Delta Plain, Louisiana, USA. *Clays and Clay Minerals*, **56**, 416–428.

Johnstone, J. (1908) *Conditions of Life in the Sea*. Cambridge University Press, Cambridge, UK, 332 pp.

Kim, J.-W., and Peacor, D.R. (2002) Crystal-size distributions of clays during episodic diagenesis: The Salton Sea geothermal system. *Clays and Clay Minerals*, **50**, 371–80.

Kim, J.-W., Peacor, D.R., Tessier, D., and Elsass, F. (1995) A technique for maintaining texture and permanent expansion of smectite interlayers for TEM observations. *Clays and Clay Minerals*, **43**, 51–57.

Kim, J.-W., Furukawa, W., Dong, H., and Newell, S.W. (2005) The role of microbial Fe(III) reduction in the clay flocculation. *Clays and Clay Minerals*, **53**, 572–579.

Kim, G.Y., Yoon, Hong J., Kim, J.-W., Kim, D.-C. Dae, Kim, B.-K., and Kim, S.-Y. (2007) The effects of microstructure on shear properties of shallow marine sediments. *Marine Georesources & Geotechnology*, **25**, 37–51.

Kretzschmar, R., Holthoff, H., and Sticher, H. (1998) Influence of pH and humic acid on coagulation kinetics of kaolinite: A dynamic light scattering study. *Journal of Colloid and Interface Science*, **202**, 95–103.

Lagaly, G. (1981) Characterization of clays by organic compounds. *Clay Minerals*, **16**, 1–21.

Lagaly, G., Barrer, R.M., and Goulding, K. (1984) Clay-organic interactions (and discussion). *Philosophical Transactions of the Royal Society (London) A14*, **311**, 315–332.

Lagaly, G. (1986) Interaction of alkylamines with different types of layered compounds. *Solid State Ionics*, **22**, 43–51.

Leppard, G.G., Heissenberger, A., and Herndl, G.J. (1996) Ultrastructure of marine snow. I. Transmission electron microscopy methodology. *Marine Ecology Progress Series*, **135**, 289–298.

Montgomery, M.T., Welshmeyer, N.A., and Kirchman, D.L. (1990) A simple assay for chitin: application to sediment trap samples from the subarctic Pacific. *Marine Ecology Progress Series*, **64**, 301–308.

Mietta, F., Chassagne, C., Manning, A.J., and Winterwerp, J.C. (2009) Influence of shear rate, organic matter content, pH and salinity on mud flocculation. *Ocean Dynamics*, **59**, 751–763.

Mietta, F., Chassagne, C., Verney, R., and Winterwerp, J.C. (2011) On the behaviour of mud floc size distribution: model calibration and model behaviour. *Ocean Dynamics*, **61**, 257–271.

O'Brien, N.R. (1971) Fabric of kaolinite and illite floccules. *Clays and Clay Minerals*, **19**, 353–359.

O'Melia, C.R. (1980) Aquasols: the behavior of small particles in aquatic systems. *Environmental Science and Technology*, **14**, 1052–1060.

Pignatello, J.J. and Day, M. (1996) Mineralization of methyl parathion insecticide in soil by hydrogen peroxide activated with iron(III)-NTA or -HEIDA complexes. *Hazardous Waste & Hazardous Materials*, **13**, 237–244.

Pinheiro, J.P., Mota, A.M., Doliveira, J.M.R., and Martinho, J.M.G. (1996) Dynamic properties of humic matter by dynamic light scattering and voltammetry. *Analytica Chimica Acta*, **329**, 15–24.

Reuter, J.H. (1977) Organic matter in estuaries. *Chesapeake Science*, **18**, 120–121.

Sloane, R.L. and Kell, T.R. (1966) The fabric of mechanically compacted kaolin. *Fourteenth National Conference on Clay and Clay Minerals*, **14**, 289–296.

Terzaghi, K. (1925) Principles of soil mechanics settlement and consolidation of clay. *Engineering News-Record*, 874–878.

Theilen, F.R. and Pecher, I.A. (1991) Assessment of shear strength of the sea bottom from shear wave velocity measurements on box cores and in-situ. Pp. 67–74 in: *Shear Wave in Marine Sediments* (J.M. Hoven *et al.*, editors). Kluwer Academic Publishers, Dordrecht, The Netherlands.

Vali, H. and Hesse, R. (1990) Alkylammonium ion treatment of clay minerals in ultrathin section: A new method for HRTEM examination of expandable layers. *American Mineralogists*, **75**, 1443–1446.

Verney, R., Lafite, R., and Brun-Cottan, J.-C. (2009) Flocculation potential of estuarine particles: The importance of environmental factors and of the spatial and seasonal variability of suspended particulate matter. *Estuaries and Coasts*, **32**, 678–693.

(*Received 7 October 2011; revised 14 February 2012; Ms. 621; A.E. R. Mikutta*)